

SAND81-0212

~~CONFIDENTIAL~~

251

SAND81-0212
Unlimited Release
UC-70

Frictional Properties of Jointed Welded Tuff

Lawrence W. Teufel

Prepared by Sandia National Laboratories, Albuquerque, New Mexico 87185
and Livermore, California 94550 for the United States Department
of Energy under Contract DE-AC04-78DP00789
Printed July 1981



Sandia National Laboratories

Issued by Sandia National Laboratories, operated for the United States Department of Energy by Sandia Corporation.

NOTICE: This report was prepared as an account of work sponsored by an agency of the United States Government. Neither the United States Government nor any agency thereof, nor any of their employees, nor any of their contractors, subcontractors, or their employees, makes any warranty, express or implied, or assumes any legal liability or responsibility for the accuracy, completeness, or usefulness of any information, apparatus, product, or process disclosed, or represents that its use would not infringe privately owned rights. Reference herein to any specific commercial product, process, or service by trade name, trademark, manufacturer, or otherwise, does not necessarily constitute or imply its endorsement, recommendation, or favoring by the United States Government, any agency thereof or any of their contractors or subcontractors. The views and opinions expressed herein do not necessarily state or reflect those of the United States Government, any agency thereof or any of their contractors or subcontractors.

Printed in the United States of America
Available from
National Technical Information Service
U. S. Department of Commerce
5285 Port Royal Road
Springfield, VA 22161
Price: Printed Copy \$4.50; Microfiche \$3.00

FRICIONAL PROPERTIES OF JOINTED WELDED TUFF*

L. W. Teufel
Sandia National Laboratories**
Albuquerque, New Mexico 87185

ABSTRACT

Successful design of an underground nuclear-waste repository in one of the welded tuff formations at the Nevada Test Site (NTS) will require a thorough understanding of the mechanical behavior of the rock mass in which the waste is to be emplaced. Field observations indicate that welded tuffs are not continuous, but form discontinuous rock masses, containing joints, faults and bedding planes. These discontinuities would be a dominant factor in controlling the structural stability of a mined repository, as well as the permeability of the surrounding rock mass. Accordingly, an extensive research program has been initiated to determine the mechanical and permeability properties of discontinuities in welded tuff.

In this report, the frictional properties of simulated (artificial) joints induced in samples of welded tuff from the Grouse Canyon Member of the Belted Range Tuff are presented as a function of normal stress, time of stationary contact, sliding velocity and degree of water saturation. Specimens consisted of right-circular cylinders with a pre-cut surface oriented at 35° to the cylinder (load) axis. Specimens were tested in triaxial compression at confining pressures to 40 MPa. The

* This work was supported by the U. S. Department of Energy (DOE) under Contract DE-ACO4-76-DPO0789.

** A U. S. DOE Facility.

coefficient of friction of the jointed tuff is independent of normal stress at a given sliding velocity. At a given normal stress, shear strength increases with increasing time of stationary contact and/or decreasing sliding velocity. The increase in friction with increasing time of contact and/or decreasing sliding velocity is consistent with a model proposed by Dieterich (1978), which suggests that increased friction is a result of an increase in the real area of contact on the sliding surface by time-dependent asperity creep. Time and velocity dependence of friction is enhanced in tuff by increasing water saturation. This behavior is attributed to increased asperity creep rate resulting from a reduction in the surface indentation hardness by stress corrosion cracking or hydrolytic weakening, both of which are enhanced by the presence of water.

TABLE OF CONTENTS

	<u>Page</u>
ABSTRACT	1-2
INTRODUCTION	9
EXPERIMENTAL PROCEDURE	10
RESULTS	11
Effect of Normal Stress	11
Time-Dependent Friction	12
Velocity Dependent Friction	13
Effect of Water	15
DISCUSSION	16
CONCLUSIONS	22
REFERENCES	23

LIST OF FIGURES

Figure 1: Photograph of simulated joint (35° precut) specimen ..	25
Figure 2: Shear stress-normal stress relation for air-dried precut joints. Plotted stress is that required for the initiation of slip	26
Figure 3: Tracing of shear stress against shear displacement for oven-dried precuts in which displacement was stopped for 60 and 2400 seconds	27
Figure 4: Plot of coefficient of friction against log time of contact for oven-dried joints	28
Figure 5: Tracing of shear stress against shear displacement in which sliding velocity was changed	29
Figure 6: Plot of coefficient of friction against log sliding velocity for oven-dried joints	30
Figure 7: Shear stress-normal stress relation for water saturated joints	31
Figure 8: Plot of coefficient of friction against log time of contact for oven-dried and water saturated joints	32

LIST OF FIGURES (Cont.)

	<u>Page</u>
Figure 9: Plot of coefficient of friction against log sliding velocity for oven-dried and water saturated joints ...	33

FRICITIONAL PROPERTIES OF JOINTED WELDED TUFF

L. W. Teufel
Sandia National Laboratories
Albuquerque, New Mexico 87185

INTRODUCTION

Extensive research is in progress to evaluate several different geologic media for the design of underground nuclear-waste repositories. Among the rock types being considered, welded tuff, which is abundant at the Nevada Test Site (NTS) (Byers, et al., 1976), is a primary candidate. The successful design of any waste repository cannot be achieved until the rock mass is adequately characterized in terms of lithology, joint systems, faults, and bedding surfaces; and until the thermomechanical response of the emplacement medium under expected conditions can be predicted reliably. More than 45 years of laboratory study of the mechanical properties of intact, homogeneous, and isotropic rock specimens have contributed greatly to our understanding of the deformations of the matrix of many rock types. However, prediction of the behavior of these same in-situ rock types, where they inherently contain joints, faults, layers of other materials, or other planes of potential mechanical discontinuity, which may be either thermal or tectonic in origin, is still very tenuous. Joints are the most pervasive fabric element that may potentially create a discontinuity in the mechanical response of a rock mass. Welded tuff formations at the Nevada Test Site are known to contain a high density of joints in some locations (see, for example, Spengler, et al., 1979; Lysman, et al., 1965). Thus, one of the first steps in assessing the rock-mass behavior of welded tuff must be the determination of the mechanical properties of joints under the appropriate environmental, loading, and boundary conditions.

In evaluating the potential response of joints to an applied load, engineers generally have considered two extreme types of joints: perfectly bonded, which is equivalent to there being no mechanical discontinuity, and unbonded, in which there is a complete lack of tensile strength. In nature, the tensile strength of a joint may not be zero, but rather some percentage of the tensile strength of the intact rock. This is especially true of mineralized or healed joints. Compressive normal stress can be transmitted across any closed joint, but the amount of shear stress transmitted across a joint will depend on the inherent shear strength and frictional properties of the joint and/or joint filling.

For an unbonded joint, the inherent shear strength is essentially zero and the shear strength is solely dependent on joint frictional properties. In this study, we present experimental results on the frictional properties of simulated, unbonded joints in the welded portion of the Grouse Canyon Member of the Belted Range tuff, collected in the G-tunnel complex on the Nevada Test Site (NTS). Results are presented as a function of normal stress, time of contact, sliding velocity, and degree of water saturation. All tests were conducted at room temperature. The effects of elevated temperature will be presented in a future report.

EXPERIMENTAL PROCEDURE

Joints were simulated in experimental samples by using right circular cylinders with a precut oriented at 35° to the cylinder (load) axis (Figure 1). The long axis of all specimens was perpendicular to bedding, and all were cored from a single block of tuff. The specimens were 4.45 cm in diameter and 12.70 cm long. The precut angle was accurate to within 0.5° for each half of the specimen. The ends of the assembled specimen were within 0.1° of parallelism. The sliding surfaces and ends of the

specimen were surface ground with an 80-grit wheel. Three Polyolefin jackets were used to isolate the specimen from the confining fluid. Lubrication in the form of a thin layer of Molykote (MoS_2) was applied to the specimen-end cap interfaces in order to maintain uniform stress distribution at the ends of the sample.

The specimens, which were laboratory air-dried, oven-dried, or water-saturated, were deformed in triaxial compression at confining pressures to 40 MPa and axial displacement rates from 10^{-2} cm/sec to 10^{-6} cm/sec. All tests were conducted at room temperature. The tests were carried out in a 1.8-GN ultra-stiff, electro-hydraulic, servo-controlled testing apparatus. Ram displacement was used as the programmed feedback variable. Axial displacement was measured by linear variable-displacement transducers mounted at two points along the length of the specimen. Transverse displacements normal to the strike of the precut slip surface were measured by a disc gage (Schuler, 1978). Both axial force and confining pressure were servo-controlled. A Digital Equipment Corp. PDP-11 was used to collect and reduce force, axial and transverse-displacement data, and to display differential stress vs. axial strain on a CRT in real time. Experimental data were stored on magnetic tape. Normal stress, shear stress, and shear displacement were calculated from the primary data.

RESULTS

Effect of Normal Stress

In order to determine the effect of normal stress on the shear stress required to initiate slip on a joint in air-dried welded tuff, room temperature tests were conducted at 5 MPa to 40 MPa confining pressure and constant sliding velocity of 1.2×10^{-4} cm/s. In these triaxial compression tests, the normal stress across the precut sliding surface was increased

by increasing the confining pressure. The shear strength of the simulated joints fit the linear relation

$$\tau = \tau_0 + \mu\sigma \quad (1)$$

as shown in Figure 2. In equation (1), τ is the shear strength, τ_0 the inherent shear strength, μ the coefficient of friction, and σ the normal stress. As indicated by the linearity of the τ , σ relation shown in Figure 2, the coefficient of friction at the initiation of slip is independent of normal stress, having a value of 0.64 at this particular sliding velocity. The independence of the coefficient of friction on normal stress is consistent with the joint-friction literature as reviewed by Byerlee (1978).

Time-Dependent Friction

Consideration of the long-term structural stability of the mined repository must be included in the design of an underground nuclear-waste facility. Accordingly, the time-dependence of the frictional shear strength of oven-dried welded tuff was investigated by examining the response of 35° precuts in triaxial compression at a confining pressure of 10 MPa. The test procedure was slightly different from that used in the previous quasi-static tests. In the tests of time-dependent behavior, axial load was increased until slip occurred along the precut at a constant sliding velocity of 1.2×10^{-3} cm/s. The test was then stopped for a given time under load, and then started again at the same sliding velocity. This procedure was repeated at several different durations of contact time.

A tracing of the change in shear stress, $\Delta\tau$, as a function of displacement (Figure 3), shows that when a test was stopped and started again after 60 seconds, there was an abrupt increase of ~ 0.4 MPa in the shear

stress necessary for slip, and then a drop back to the former stress level, as slip continued at the previous sliding velocity of 1.2×10^{-3} cm/s (Figure 3). With a longer time of stationary contact (2400 seconds) both the stress rise required to initiate slip and the corresponding stress drop were larger; the stress required for stable sliding did not change significantly.

A plot of the coefficient of friction at peak stress, μ , versus the log time of contact (Figure 4) shows that with increasing time of contact there was a consistent increase in the friction required to initiate sliding. A linear fit to this data can be made using the empirical equation

$$\mu = \mu_0 + A \log(Bt + 1) \quad , \quad (2)$$

from Dieterich (1978). In this equation μ_0 is the friction at constant sliding velocity, t is time of stationary contact in seconds and A and B are experimentally determined constants. For the oven-dried welded tuff studied here μ_0 is 0.63, A is 0.014, and B is 1. Dieterich (1978) found the constant A to be 0.016, 0.022, 0.020, and 0.012 for joints in sandstone, granite, quartzite, and graywacke, respectively. Average values of μ_0 in Dieterich's study ranged from 0.7 to 0.8 and B was approximately equal to 1. Dieterich found these parameters to be insensitive to normal stress. Experiments are planned at various normal stress conditions to determine if the time-dependent frictional properties of tuff are also independent of normal stress.

Velocity Dependent Friction

The time dependence of the static-friction coefficient of joints in oven-dried welded tuff suggests the possibility of a velocity dependence

as well. In order to determine if a variation in the sliding velocity affected the frictional resistance, a series of tests were conducted in which the sliding velocity was abruptly changed during sliding. A tracing of changes in shear stress, $\Delta\tau$, against displacement is shown in Figure 5. As the velocity was decreased from 1.2×10^{-4} cm/s to 1.2×10^{-5} cm/s, there was a small drop and then an increase in the shear stress required for stable sliding. When sliding was allowed to occur at this slower velocity for a small amount of displacement and then the sliding velocity was abruptly increased to 1.2×10^{-3} cm/s, there was a sudden rise, and then a drop in the shear stress at stable sliding to a lower level characteristic of the faster velocity.

When the sliding velocity was changed, the frictional resistance did not change immediately to the new steady state value. In all cases, as the velocity was increased or decreased, a small but measurable displacement was required before the shear stress stabilized at a value characteristic of the new sliding velocity. This critical displacement, d_c , was consistent, ranging from 6 to 13 μm , with an average value of 8 μm .

Dieterich (1978) also observed this displacement phenomenon in experiments on Westerly granite. He found the critical displacement to be independent of machine effect and normal stress, but dependent on surface roughness. An increase in surface roughness required a larger critical displacement. Hence, Dieterich suggested that d_c was an intrinsic quality of the sliding surface.

A plot of the coefficient of friction, μ , versus log sliding velocity shows that μ for the dry joints decreased with increasing velocity toward an asymptotic value near 0.62 (Figure 6). Following Dieterich (1978), an equation

$$\mu = \mu_0 + A \log \left(B \frac{d_c}{v} + 1 \right) \quad (3)$$

can be fit to the data. In equation (3), μ_0 , A, and B are the same constants as in the previous time-of-contact fit (equation (2)), d_c is the average critical displacement, and v is the sliding velocity. Note that equations (2) and (3) are different only in that time, t , in (2) has been replaced by $\frac{d_c}{v}$ in (3). A detailed explanation of the time and velocity dependent equations is given in the discussion section.

Effect of Water

Current plans indicate that a repository in welded tuff would be positioned below the water table. Thus, the potential effects of water on the frictional properties of jointed tuff need to be evaluated. Accordingly, a series of tests was conducted on water-saturated 35° precuts at confining pressures from 5 to 40 MPa and constant sliding velocity of 1.2×10^{-4} cm/s. As in the case of dry tuff, the coefficient of friction for wet tuff is independent of normal stress (Figure 7). The coefficient of friction, μ , of wet tuff is 9 percent greater than dry tuff, having a value of 0.70. Thus, at a given normal stress, a saturated joint is slightly stronger than a dry one.

The relative increase in frictional resistance of joints in welded tuff due to water saturation is enhanced as the time of stationary contact increases (Figure 8). As with dry tuff, an empirical fit to the wet data using equation (2) can be made for the saturated joint with μ_0 equal to 0.68, A equal to 0.022 and B equal to 1. In this empirical fit, the increased time-dependence of a wet joint relative to a dry joint is reflected by the parameter A, which is 57 percent greater for the wet tuff.

An analogous increased velocity dependence of the coefficient of friction for a joint in wet tuff relative to dry tuff was also observed (Figure 9). A fit to the wet data can be made using equation (3) with d_c being the same as for dry tuff ($8 \mu\text{m}$) and μ_0 , A and B the same as for the previous time-of-contact fit for water-saturated welded tuff. The separation of divergence between the two curves shown in Figure 9 is thus a result of differing coefficient of friction at high sliding velocities (μ_0), and the differing time-dependent behavior (as reflected in the constant A).

DISCUSSION

In the design of underground excavations in jointed rock masses, engineers have generally assumed that the coefficient of friction of joints increases only with increasing surface roughness (Barton, 1976). In general, however, the effect of surface roughness has been found to be important only at low normal stresses and is a result of interlocking of asperities on the sliding surface. Quasi-static experiments on a variety of jointed rock types with extreme variation in surface roughness have shown that μ can range from 0.4 to 10 at normal stresses less than 10 MPa (Barton, 1976). At higher normal stresses, surface roughness is not a significant factor, since asperities are sheared off by cataclasis and incorporated into gouge along the sliding surface. Quasi-static test measurements of μ compiled by Byerlee (1978) for joints of differing surface roughnesses in a wide variety of rock types indicate a range of μ from 0.4 to 1.0 at normal stresses greater than 10 MPa. The results of this experimental study on simulated joints in welded tuff are consistent with this in that the normal stresses across joints were 8-70 MPa,

and all measured values of μ were less than 1.0. The confining pressure, generally 10 MPa, is representative of emplacement at a depth of some 1500 feet. Likely emplacement depths in welded tuff range from 1000 to 3000 feet.

In modeling the long-term stability of a jointed rock mass around an underground opening, engineers have further assumed that μ for joints with a particular surface roughness is a constant and that quasi-static friction measurements of μ are sufficient input for modeling purposes. However, the results of this experimental study have shown that μ of joints in welded tuff is not a constant, but increases with increasing time of stationary contact and/or decreasing sliding velocity.

Two observational studies have attributed time-dependent increase of friction in jointed rocks to growth of asperity contacts by creep (Scholz and Engelder, 1976; Teufel and Logan, 1978). Their observations are similar to those for friction of metal (Bowden and Tabor, 1954). The model for time dependence in metals contends that the frictional force necessary for slip is the force required to shear the junctions at asperity contacts on the sliding surface. If the asperity contact deforms by a creep mechanism such that the size of the junctions increase with time, the real area of contact and frictional resistance to slip also increase.

Dieterich (1978) extended this frictional model and established a common basis for static and sliding friction, based on the interaction between time, displacement, and velocity dependence on friction. Dieterich suggested that, in the absence of time-dependent friction effects due to asperity creep, the static and sliding coefficient of friction are equal to the same constant value. However, as a result of time-dependent creep of asperity contacts, there is an increase in the coefficient of friction

above this constant value with increasing time of stationary contact and/or decreased sliding velocity. This increased frictional resistance is proportional to the logarithm of the time that a population of asperity contacts on the sliding surface (real area of contact) exists. For static friction, the lifetime of an asperity contact population is simply the time of stationary contact. For sliding friction, the population of asperity contacts is continuously changing in response to changes in displacement; the time of contact is therefore a function of the sliding velocity and the critical displacement required to change the population of asperity contacts. Accordingly, Dieterich interpreted the measured critical displacement parameter, d_c , in the variable-velocity experiments to represent the displacement required to eliminate the population of contacts characteristic of a previous velocity.

Thus, velocity dependent friction is a result of two distinct and competing factors. First, as a population of contacts ages, the shear stress required to initiate sliding increases according to equation (2). The time allowed for this process is inversely proportional to the sliding velocity. Second, displacement causes the destruction of older and hence stronger contacts which are then replaced by new and consequently weaker contacts. Velocity dependent friction is therefore formally analogous to time-dependent friction with time, t , being replaced by d_c/v , where d_c is the measured critical displacement and v is the sliding velocity. Consequently, the equations describing the time and velocity dependence for friction, (2) and (3) respectively, are identical provided that the parameters, μ_0 , A and B are the same.

The application of Dieterich's friction model to both oven-dried and water-saturated welded tuff has been highly successful in this study.

Moreover, in fitting the experimental data to Dieterich's model, the increased time and velocity dependence in friction for wet joints relative to dry surfaces is solely reflected by a parameter A in equations (2) and (3). The parameter A increases from 0.014 for dry tuff to 0.022 for wet tuff, an increase of 57 percent. It is suggested that the enhanced time-dependent increase in friction due to the presence of water is a result of an increase in the creep rate at asperity contacts. It is also suggested that parameter A in equations (2) and (3) is an indirect measure of the asperity creep rate.

Several studies (for example, Scholz and Engelder, 1976; Teufel and Logan, 1978) have suggested that the mechanism for asperity creep and time-dependent friction is time-dependent reduction of surface hardness at asperity contact junctions by dislocation mobility and the propagation of cracks. Water is known to enhance dislocation mobility in silicate minerals by hydrolytic weakening, a mechanism of hydration and breaking of Si-O bonds at dislocation cores (Griggs and Blacic, 1965). Studies on stress corrosion cracking in metals and nonmetallic crystalline solids (including quartz and calcite) have also indicated a role for water in assisting to break atomic bonds at crack tips and enhance crack propagation (Anderson and Grew, 1977). Both hydrolytic weakening and stress-corrosion cracking can reduce the failure and yield strength of a material and also increase the creep rate. Olsson (1981) has recently shown a 30 percent reduction in the unconfined, compressive strength of welded samples from the Grouse Canyon Member of the Belted Range Tuff, due to water saturation. In addition, Westbrook and Jorgensen (1965) have shown that the observed reduction of the surface hardness of nonmetallic minerals by creep under atmospheric conditions is caused by absorbed water. They have demonstrated that the reduction in

surface hardness is reduced or eliminated when the minerals are tested in a water-free environment following heating to 300°C in an argon atmosphere to remove absorbed water.

These studies support the observations of increased asperity creep and time-dependent friction of joints in welded tuff in water-saturated environments. Furthermore, the work of Westbrook and Jorgensen suggests that even for oven-dried tuff specimens (100°C for 24 hours), there is sufficient absorbed water on the sliding surface to cause time-dependent asperity creep and frictional resistance. To further examine the effect of water on time-dependent friction, time-of-contact friction experiments are planned in which the specimens will be oven-dried (100°C for 24 hours) under a vacuum and then flushed with argon gas to eliminate the absorbed water. If water is a critical parameter in reducing surface hardness and increasing asperity creep, these tests should show little or no increase in the coefficient of friction with increasing time of contact.

The effect of water on time-dependent friction and reduction of surface hardness is only one of the larger class of changes in mechanical and surface properties induced by chemical surfactants. Several studies (for example, Westwood, et al., 1967; MacMillian, et al., 1974) have shown that in chemically active environments there is a direct correlation between the near-surface zeta potential, material properties (including failure strength, yield strength, and indentation hardness) and dislocation mobility. At zero zeta potential, the near-surface dislocation mobility is at a minimum and the surface and mechanical strength properties are at a maximum. The zeta potential is the electrical potential at the boundary between the inner absorbed layer and the outer diffuse layer of ions on the surface. The zeta potential may be controlled by highly charged complex

ions, or by organic molecules possessing a high dipole moment. An example of the effect of chemically active surfactants on indentation creep (reduction in surface hardness) and friction is presented by MacMillian, et al., (1974). This study shows that for MgO and soda-lime glass in a chemically active environment with a higher zeta potential than water, there is an increase in the time-dependent dislocation mobility of the surface, and consequently a larger reduction in surface hardness and a higher frictional resistance than in a water environment. Accordingly, these studies suggest that the mechanical and frictional properties of tuff in a more chemically active environment than pure water may display a larger increase in time-dependent friction for jointed tuff, a larger reduction in the failure strength, and an increased creep rate for intact tuff than seen here. It is suggested that future tests be conducted using ground water from a possible repository horizon, in order to better determine site-specific time-dependent mechanical properties of jointed and intact welded tuff.

The time-dependence of friction of joints in welded tuff may not only affect the strength of jointed tuff, but also the permeability, since asperity creep on the joint surface may result in joint healing or closure. The critical parameter for joint permeability is the aperture of the joint. Joint aperture is generally considered to be a function only of the joint surface roughness and normal stress. For a given surface roughness, the aperture decreases with increasing normal stress. However, if joint closure also occurs as a result of time-dependent asperity creep, then the permeability of the joint will also decrease with time. Accordingly, it is suggested that permeability experiments on jointed tuff be conducted as a function of surface roughness and normal stress over long time periods (3

months) in order to determine time-dependent joint permeability. Variations in water chemistry may also affect asperity creep and joint closure, and hence, permeability, and should be considered.

CONCLUSIONS

The results of the experiments on simulated joints in welded tuff from the Grouse Canyon Member of the Belted Range Tuff warrant the following conclusions:

1. The coefficient of friction of the joints is independent of normal stress at a given sliding velocity.
2. The coefficient of friction increases with both increasing time of stationary contact and decreasing sliding velocity.
3. Time and velocity dependence of friction is due to an increase in the real area of contact on the sliding surface, caused by asperity creep.
4. Joints in water-saturated tuff show a greater time and velocity dependence of friction than those in dehydrated tuff.
5. The enhanced time and velocity dependence of friction with water saturation is a result of increased creep at asperity contacts, which is in turn due to a reduction in the surface indentation hardness by hydrolytic weakening and/or stress corrosion cracking.

REFERENCES

1. Anderson, D. L. and Grew, P. C. (1977), Stress corrosion theory of crack propagation with applications to geophysics. *Rev. Geophys. Space Phys.*, 7, 77-104.
2. Barton, M. (1973), Review of new shear strength criterion for rock joints. *Eng. Geol.*, 7, 287-332.
3. Bowden, F. P. and Tabor, D. (1950), *The friction and lubrication of solids*. Oxford Univ. Press, Oxford, p. 337.
4. Eyerlee, J. (1978), Friction of rocks. *Pageoph*, 116, 615-626.
5. Byers, F. J., Carr, W. J., Orkild, P. R., Quianlivan, W. D. and Sargent, K. A. (1976), Volcanic suite and related cauldrons of Timber Mountain-Oasis Valley Cauldron Complex, Southern Nevada. USGS Prof. Paper 919.
6. Dieterich, J. H. (1978), Time-dependent friction and the mechanics of stick-slip. *Science*, 147, 292-295.
7. Griggs, D. T. and Blacic, J. D. (1965), Quartz: Anomalous weakness of synthetic crystals. *Science*, 147, 292-295.
8. Lipman, P. W., Christiansen, R. L. and O'Connor, J. T. (1966), A compositionally zoned ash-fall sheet in southern Nevada. USGS Prof. Paper 424-F.
9. MacMillian, N. H., Huntington, R. D. and Westwood, A. R. C. (1974), Chemomechanical control of sliding friction in nonmetals. *Jour. Materials Science*, 9, 697-706.
10. Olsson, W. A. (1980), Rock mechanics properties of volcanic tuffs from the Nevada Test Site, Sandia National Laboratories Report SAND80-1453, Sandia National Laboratories, Albuquerque, NM 87185.
11. Scholz, C. H. and Engelder, J. T. (1976), The role of asperity indentation and ploughing in rock friction: I. Asperity creep and stick-slip. *Int. J. Rock Mech. Min. Sci. and Geomech. Abstr.*, 13, 149-154.
12. Schuler, K. W. (1978), Lateral-deformation gage for rock mechanics testing. *Exp. Mech.*, 18, 477-480.
13. Spengler, R. W., Muller, D. C. and Livermore, R. B. (1979), Preliminary report on geology and geophysics of drill hole UE25a-1, Yucca Mountain, Nevada Test Site. USGS Open-File Report 79-1244.
14. Teufel, L. W. and Logan, J. M. (1978), Effect of displacement rate on the real area of contact and temperatures generated during frictional sliding of Tennessee sandstone. *Pageoph*, 116, 825-840.

15. Westbrook, J. H. and Jorgensen, P. J. (1965), Indentation creep of solids. *Trans. Amer. Inst. Min. Met. Engr.*, 233, 425-428.
16. Westwood, A. R. C., Goldheim, D. L. and Lye, R. G. (1967), Rebinder effects in MgO. *Phil. Mag.* 16, No. 141, 505-519.

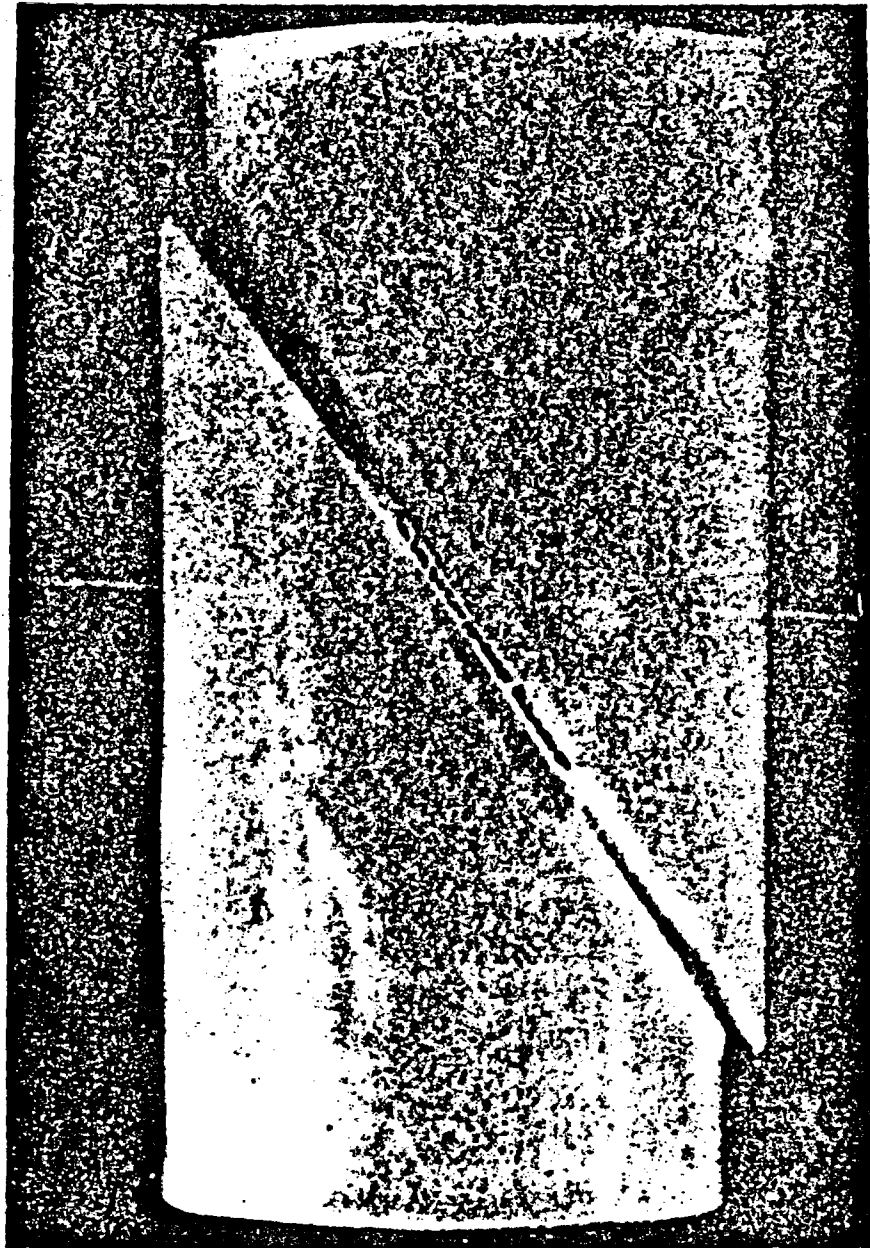


Figure 1: Photograph of simulated joint (35° precut) specimen

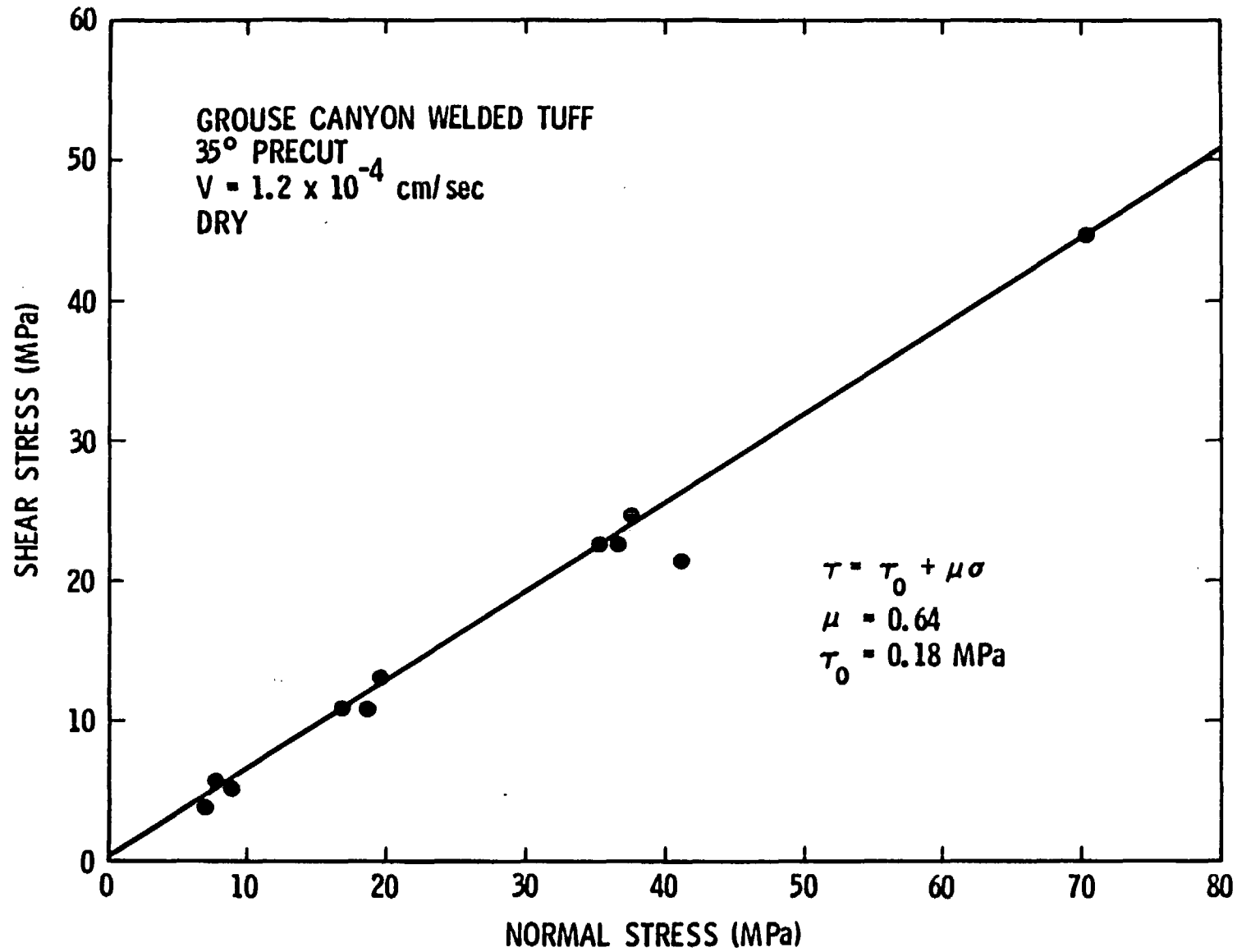


Figure 2: Shear stress-normal stress relation for air-dried precut joints. Plotted stress is that required for the initiation of slip.

GROUSE CANYON WELDED TUFF
35° PRECUT
 $P_c = 10 \text{ MPa}$
DRY

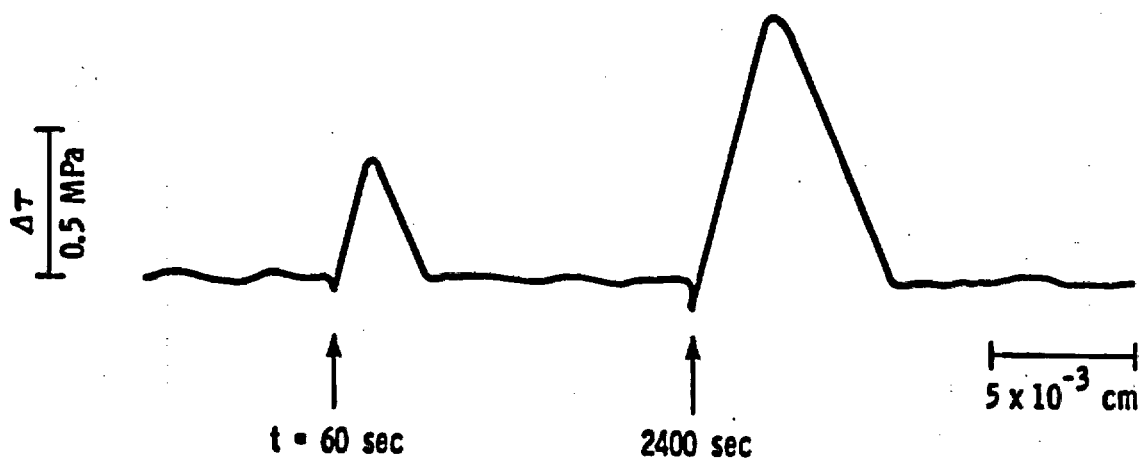


Figure 3: Tracing of shear stress against shear displacement for even-dried precuts in which displacement was stopped for 60 and 2400 seconds.

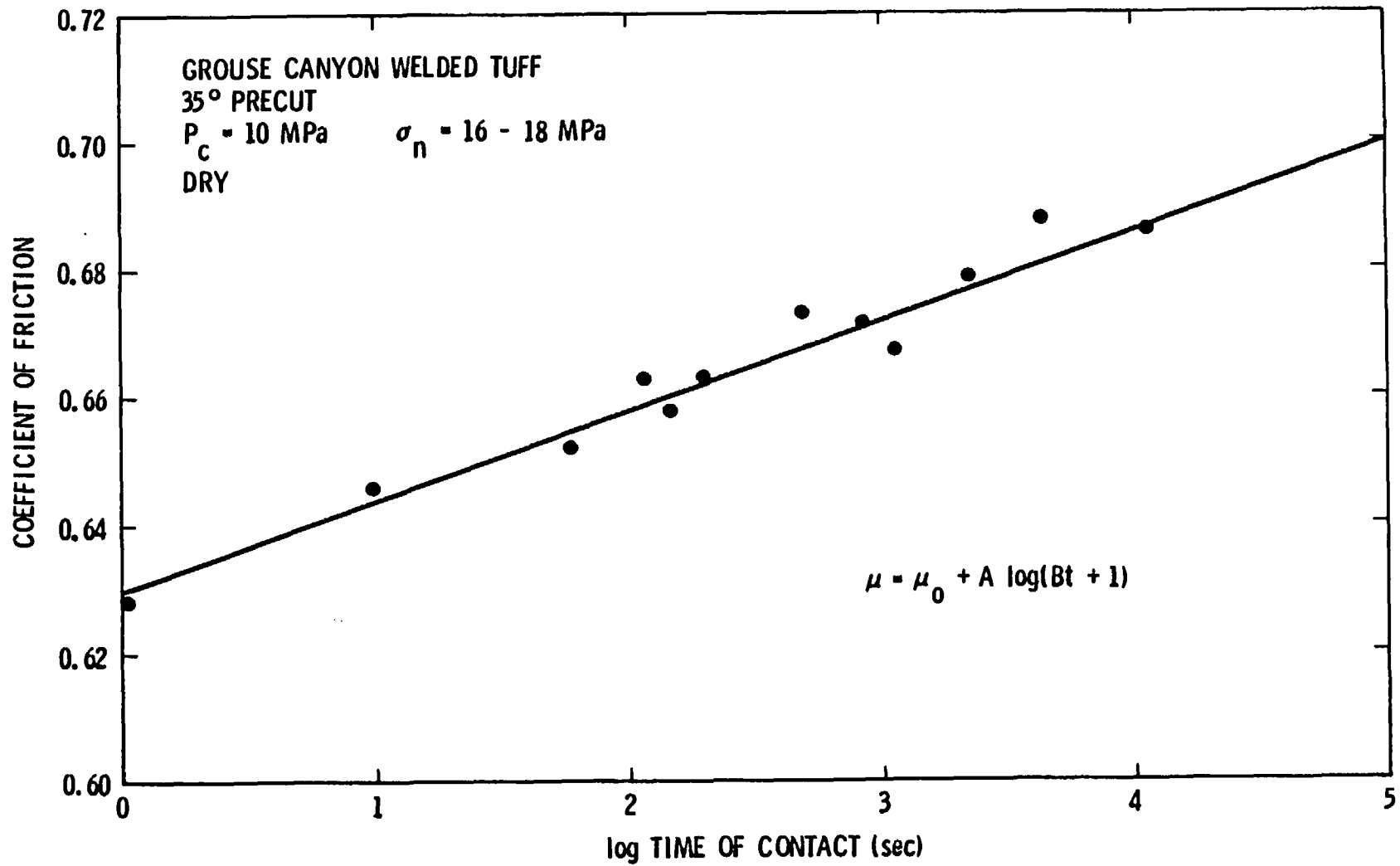


Figure 4: Plot of coefficient of friction against log time of contact for oven-dried joints.

GROUSE CANYON WELDED TUFF
35° PRECUT
 $P_c = 5 \text{ MPa}$
DRY

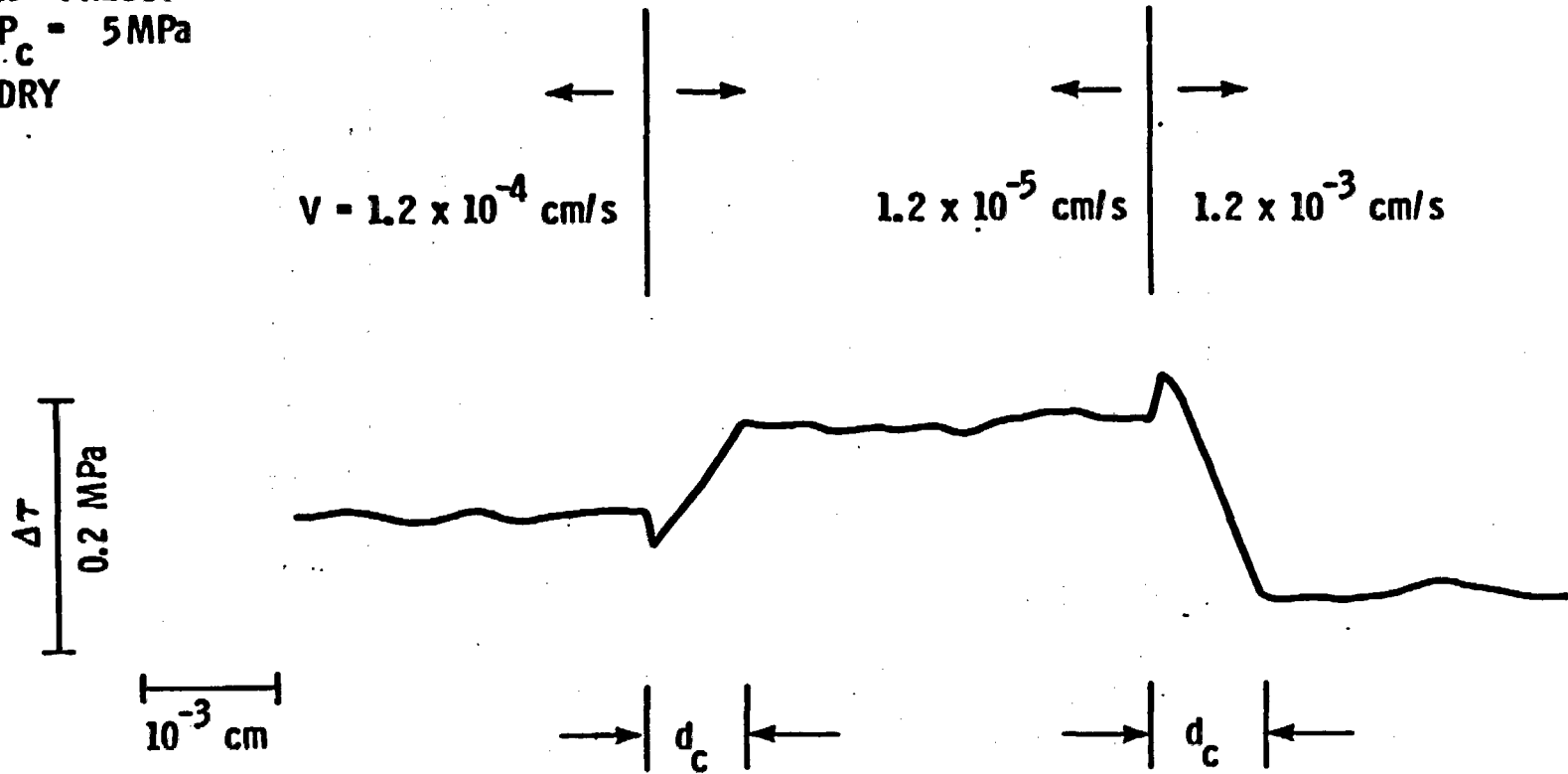


Figure 5: Tracing of shear stress against shear displacement in which sliding velocity has changed.

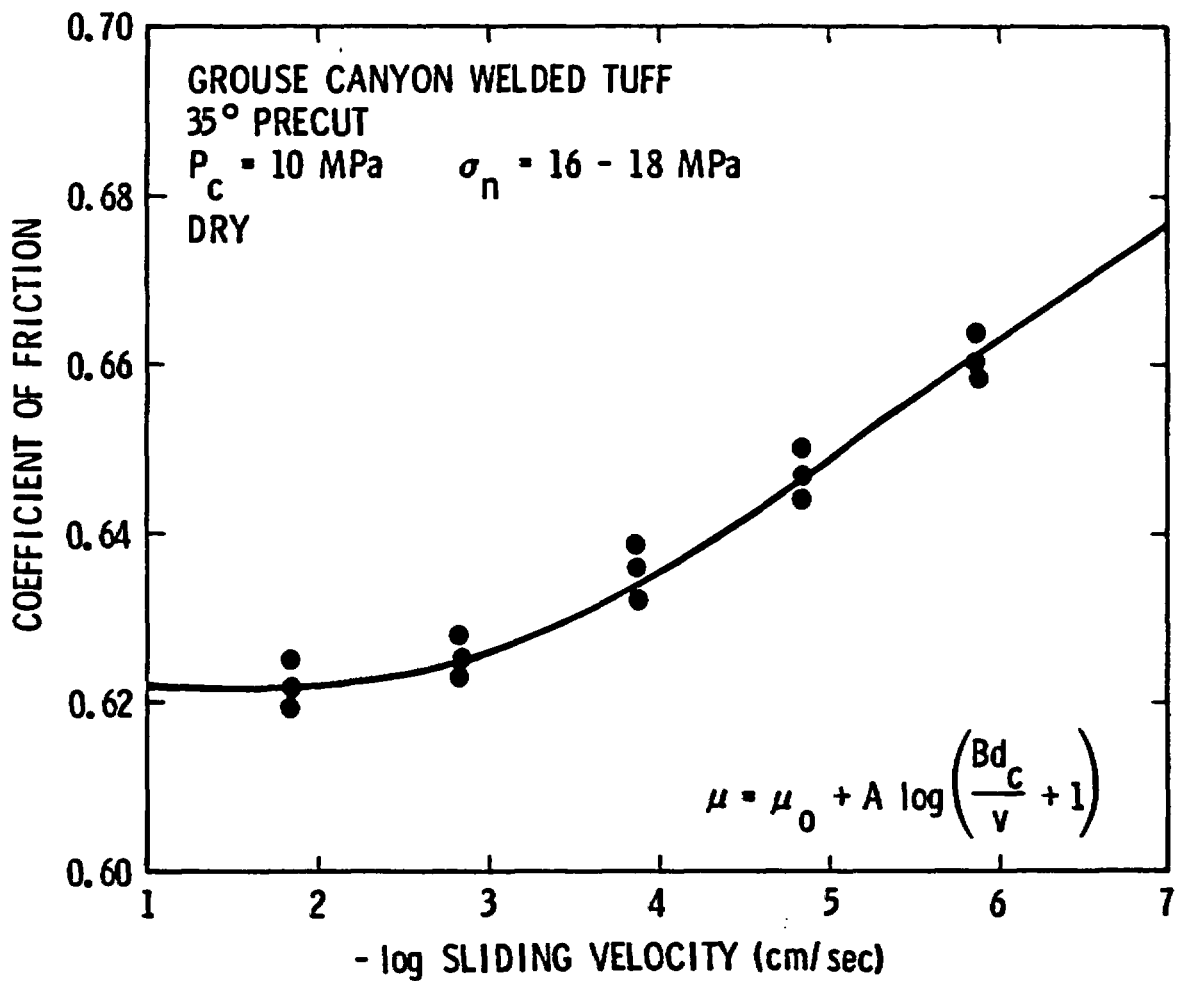


Figure 6: Plot of coefficient of friction against log sliding velocity for oven-dried joints.

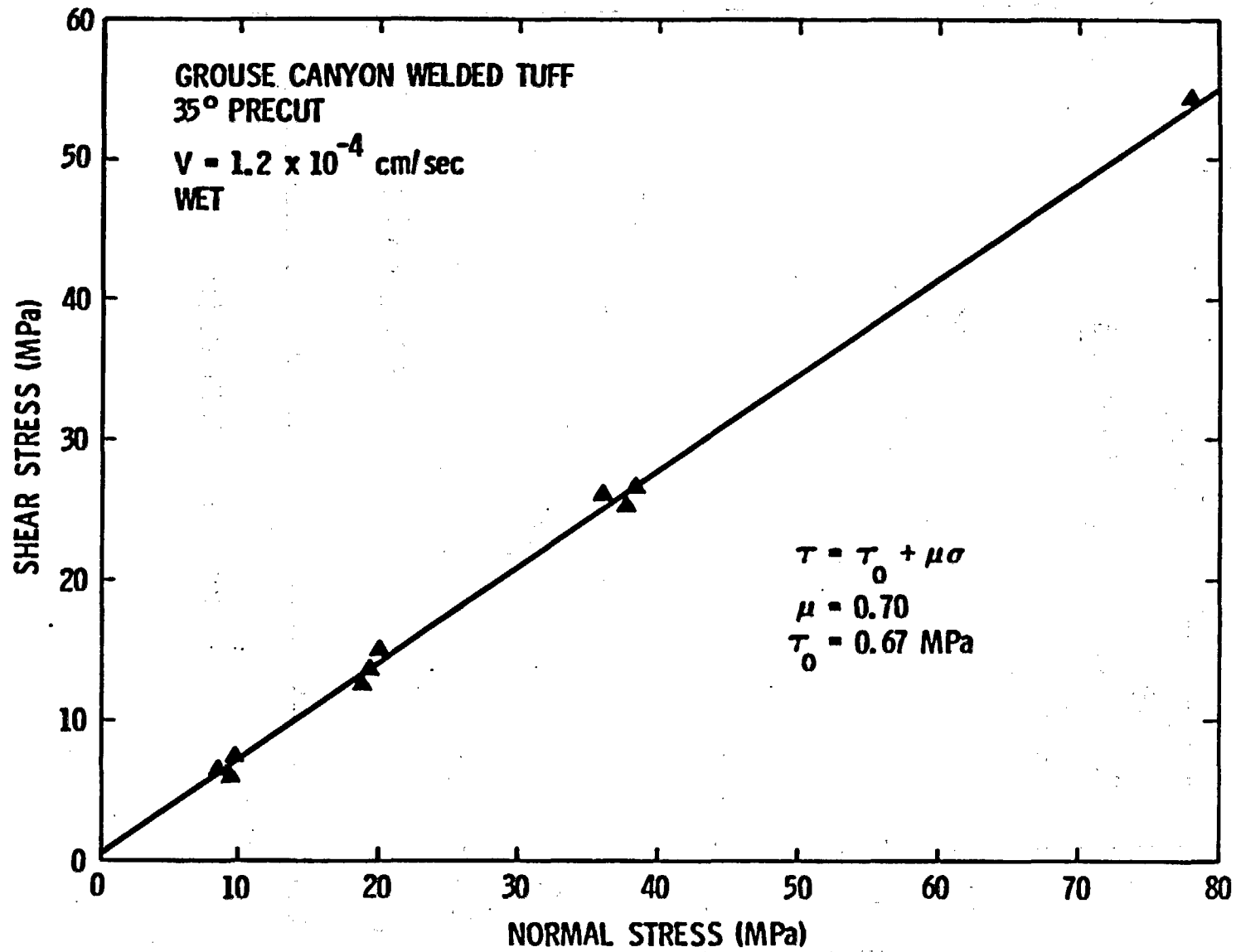


Figure 7: Shear stress-normal stress relation for water saturated joints.

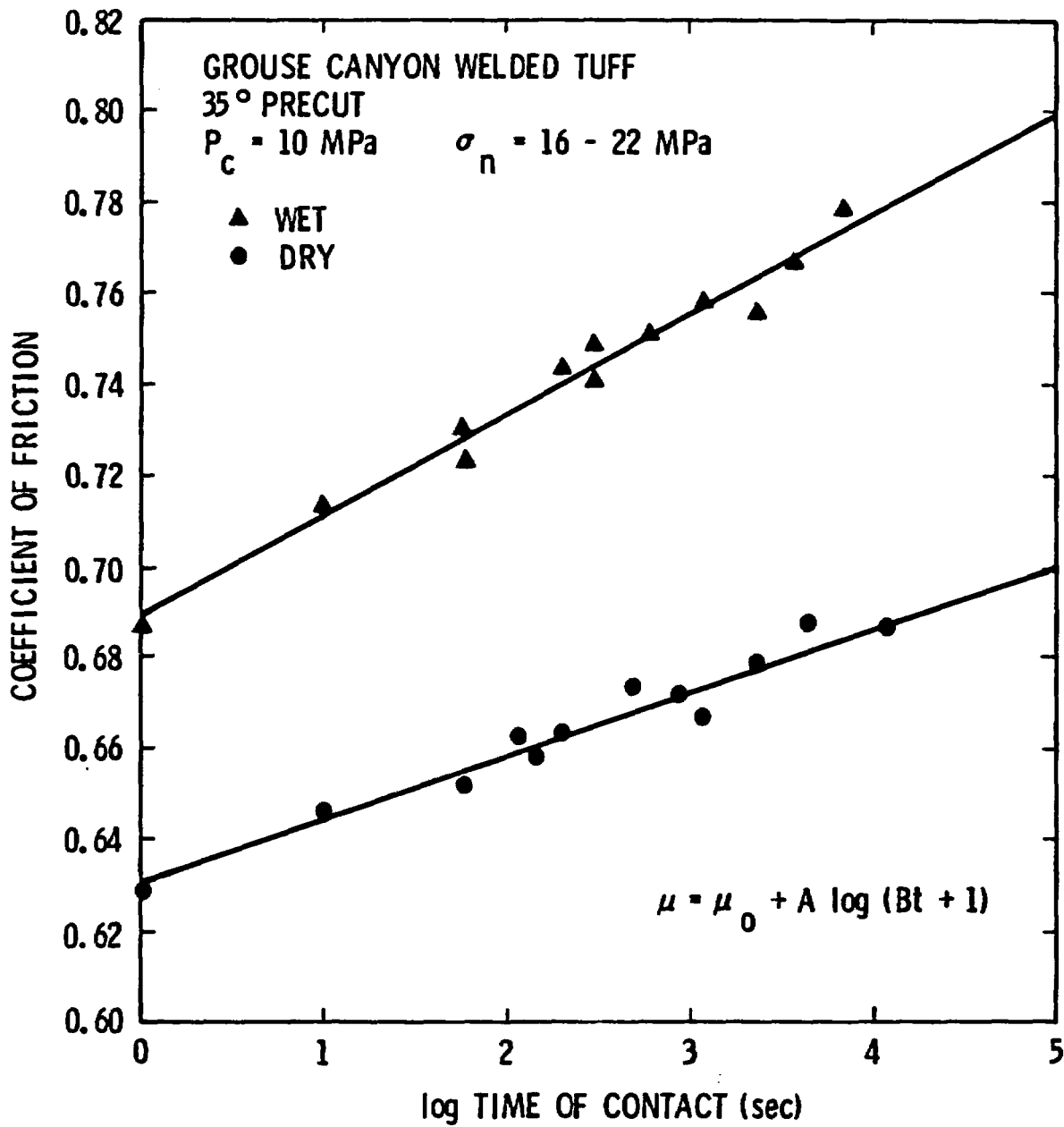


Figure 8: Plot of coefficient of friction against log time of contact for oven-dried and water saturated joints.

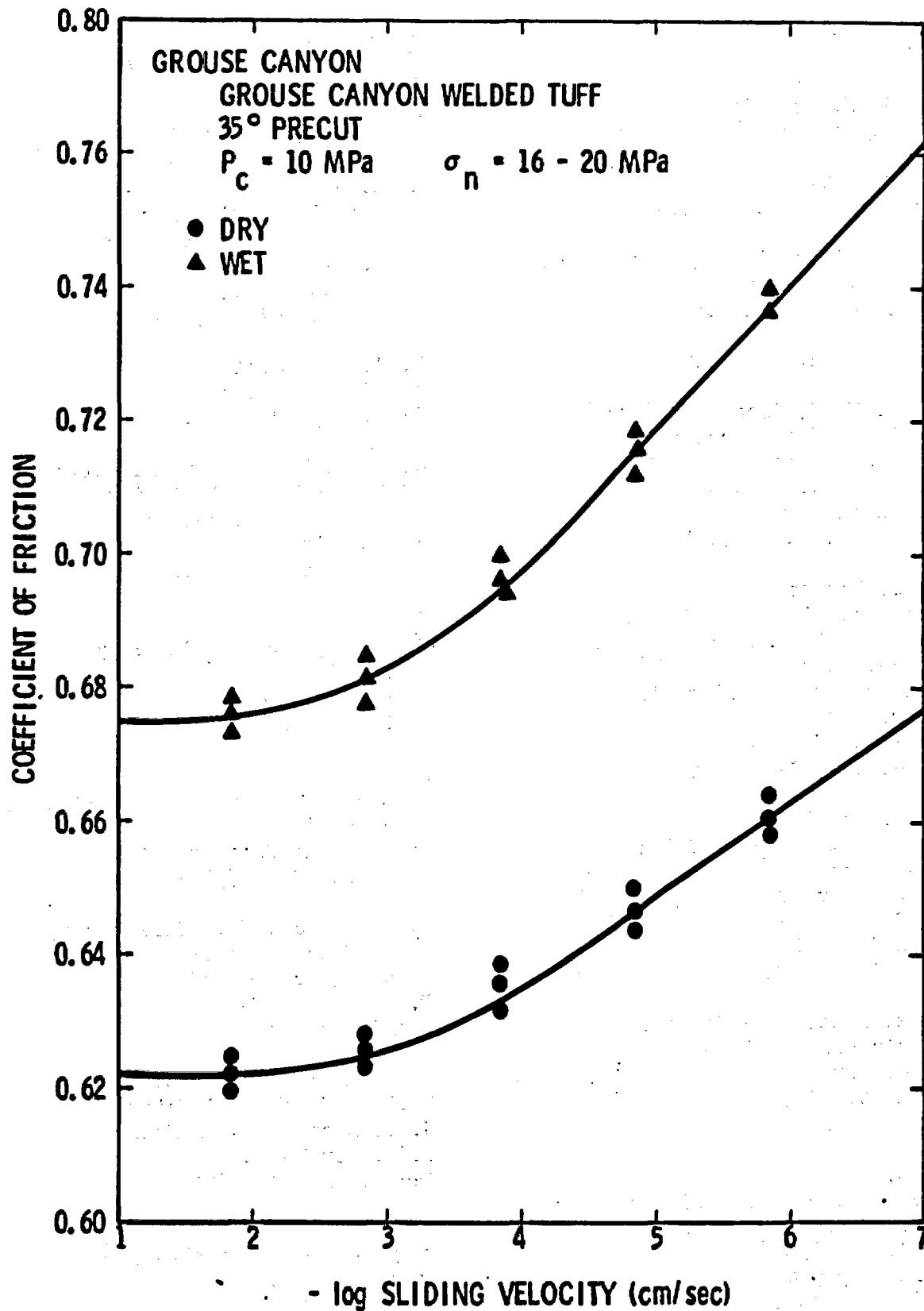


Figure 9: Plot of coefficient of friction against log sliding velocity for oven-dried and water saturated joints.

Distribution:

UC-70

C. A. Heath, Director
Office of Waste Isolation
U. S. Department of Energy
Room B-207
Germantown, MD 20767

D. L. Vieth, Acting Team Leader
Technology Team
U. S. Department of Energy
Room B-220
Germantown, MD 20767

J. O. Neff, Program Manager
National Waste Terminal
Storage Program Office
U. S. Department of Energy
505 King Avenue
Columbus, OH 43201

L. D. Ramspott
Technical Project Officer
Lawrence Livermore National
Laboratory
University of California
P. O. Box 808
Mail Stop L-204
Livermore, CA 94550

B. R. Erdal
Technical Project Officer
Los Alamos National Laboratory
University of California
P. O. Box 1663
Mail Stop 514
Los Alamos, NM 87545

A. R. Hakl, Site Manager
Westinghouse - AESD
P. O. Box 708
Mail Stop 703
Mercury, NV 89023

G. L. Dixon
Technical Project Officer
U. S. Geological Survey
P. O. Box 25046
Mail Stop 954
Federal Center
Denver, CO 80301

W. E. Wilson
U. S. Geological Survey
P. O. Box 25046
Mail Stop 954
Denver, CO 80301

A. E. Stephenson
Technical Overview Management
Sandia National Laboratories
P. O. Box 14100
Organization 4538
Las Vegas, NV 89114

W. S. Twenhofel
820 Estes Street
Lakewood, CO 80226

C. R. Cooley, Deputy Director
Office of Waste Isolation
U. S. Department of Energy
Room B-214
Germantown, MD 20767

R. G. Goranson
U. S. Department of Energy
Richland Operations Office
P. O. Box 550
Richland, WA 99352

R. Deju
Rockwell International Atomic Inter-
national Division
Rockwell Hanford Operations
Richland, WA 99352

R. M. Nelson, Jr., Director (3)
Waste Management Project Office
U. S. Department of Energy
P. O. Box 14100
Las Vegas, NV 89114

D. F. Miller, Director
Office of Public Affairs
U. S. Department of Energy
P. O. Box 14100
Las Vegas, NV 89114

R. H. Marks
U. S. Department of Energy
CP-1, M/S 210
P. O. Box 14100
Las Vegas, NV 89114

B. W. Church, Director
Health Physics Division
U. S. Department of Energy
P. O. Box 14100
Las Vegas, NV 89114

R. R. Loux (7)
U. S. Department of Energy
P. O. Box 14100
Las Vegas, NV 89114

A. E. Gurrola
Holmes & Barver, Inc.
P. O. Box 14340
Las Vegas, NV 89114

K. Street, Jr.
Lawrence Livermore National
Laboratory
University of California
Mail Stop L-209
P. O. Box 808
Livermore, CA 94550

D. C. Hoffman
Los Alamos National Laboratory
Mail Stop 760
P. O. Box 1663
Los Alamos, NM 87545

N. E. Carter
Battelle
Office of Nuclear Waste Isolation
505 King Avenue
Columbus, OH 43201

W. A. Carbiener
Battelle
Office of NWTIS Integration
505 King Avenue
Columbus, OH 43201

S. Goldsmith
Battelle
Office of Nuclear Waste Isolation
505 King Avenue
Columbus, OH 43201

ONWI Library (5)
Battelle
Office of Nuclear Waste Isolation
505 King Avenue
Columbus, OH 43201

R. M. Hill
State Planning Coordinator
Governor's Office of Planning
Coordination
State of Nevada
Capitol Complex
Carson City, NV 89023

N. A. Clark
Department of Energy
State of Nevada
Capitol Complex
Carson City, NV 89710

J. P. Colton
International Atomic Energy Agency
Division of Nuclear Power & Reactors
Karnter Ring 11
P. O. Box 590, A-1011
Vienna, Austria

H. D. Cunningham
Reynolds Electrical & Engineering
Co., Inc.
Mail Stop 555
P. O. Box 14400
Las Vegas, NV 89114

J. A. Cross
Fenix & Scisson, Inc.
P. O. Box 15408
Las Vegas, NV 89114

A. M. Friedman
Argonne National Laboratories
9700 S. Cass Avenue
Argonne, IL 60439

1417 F. W. Muller
1417 G. F. Rudolfo (2)
4500 E. H. Beckner
4510 W. D. Weart
4512 T. O. Hunter
4530 R. W. Lynch
4531 L. W. Scully
4537 L. D. Tyler (7)
4538 R. C. Lincoln (7)
4540 M. L. Kramm
4550 R. M. Jefferson
5500 O. E. Jones
5510 D. B. Hayes
5511 J. W. Nunziato
5520 T. B. Lane

5521 L. W. Davison
5521 R. K. Thomas
5530 W. Herrmann
5532 B. M. Butcher
5532 D. J. Holcomb
5532 W. A. Olsson
5532 L. W. Teufel (20)
5532 R. H. Price
5541 W. C. Luth
3141 L. J. Erickson (5)
3154-3 C. H. Dalin (20)
8214 M. A. Pound

